Available online at www.sciencedirect.com

SCIENCE DIRECT®

Surface & Coatings Technology 194 (2005) 300–318

SURFACE & COATINGS TECHNOLOGY

www.elsevier.com/locate/surfcoat

Characterization of cascade arc assisted CVD diamond-coating technology: Part II. Coating properties and applications

Vladimir I. Gorokhovsky*

Arcomac Surface Engineering, LLC., Bozeman, MT, USA

Received 9 January 2004; accepted in revised form 23 August 2004
Available online 10 November 2004

Abstract

The cascade arc assisted chemical vapor deposition (CACVD) reactor is capable of producing high-quality diamond coatings to accommodate high-volume production. This reactor has demonstrated the ability to deposit polycrystalline diamond coatings with high uniformity and industrial-scale productivity. Precise control of plasma parameters as well as thermal management of substrates allows for optimization of coating deposition on substrates of different materials having various geometries. Approximately 1000 cylindrical substrates 2 mm diameter×20 mm long can be mounted and coated simultaneously in the industrial tubular CACVD reactor with 1-m-long reaction zone. The coating properties were studied by electron microscopy and Raman spectroscopy. The influence of various predeposition treatments on coating properties was investigated. A comparison of characteristics of films deposited on carbide, Mo, W and stainless steel substrates is also presented. The correlation between the morphology of CVD diamond coatings vs. substrate material and its position in the reactor chamber was assessed using micro-Raman spectroscopy and secondary electron microscopy. There was no indication to suggest the relationship between the substrate position in the reactor and coating properties.

Keywords: Cascade arc; Diamond coatings; Substrates; Carbide inserts; Dental burs; SEM; Raman spectroscopy

1. Introduction

Diamond coatings have been deposited from Ar–CH_4–H_2 arc plasma for more than 15 years. Arc plasma discharge provides high ionization and dissociation rates resulting in the generation of intensive fluxes of reaction species. The unique advantages and features of the cascade arc assisted chemical vapor deposition (CACVD) process for the deposition of diamond coatings were described in Part I of this paper. As opposed to the conventional arc jet CVD technology, in the CACVD process substrates can be installed adjacent to the arc plasma column, forming a channel for a wall-stabilized cascade arc discharge with virtually unlimited length. In this arrangement, the substrates are not subjected to direct hydrodynamic impact by the plasma stream. The distribution of plasma temperature and concentrations of reaction species is uniform along the axis of the reactor. At the same time, a sharp transversal gradient of plasma temperature and electron density generates an intensive side flow of reaction species toward substrates to be coated positioned along the reactor wall. In a CACVD reactor, substrates are inherently biased relative to surrounding plasma environment with bias voltage of about 10–20 V similar to other plasma-assisted technologies [5,6]. The substrate bias voltage can be increased by applying additional DC or AC potentials. Substrate bias is a known factor influencing the nucleation density of diamond crystals and quality of diamond films [2,3]. An external longitudinal magnetic field is imposed to increase the concentration of excited atoms and molecules in the arc plasma environment. A transversal rotational magnetic field moves the plasma column around the axis of the reactor channel effectively activating the reaction environment near the substrate installation zone.

* Tel.: +1 406 522 7620; fax: +1 406 522 7617.
E-mail address: vigase@aol.com.

0257-8972/$ - see front matter © 2004 Elsevier B.V. All rights reserved.
doi:10.1016/j.surfcoat.2004.08.209

In the present work, a number of diamond coatings were deposited on substrates of various geometries composed of stainless steel, tungsten, molybdenum and tungsten carbide in two CACVD reactors. A novel composite powder variable conductance insulation (CPVCI) technique was used for thermal management of the substrates in the CACVD processes [31] (see also Part I of this paper). The purpose of the work was to investigate coating properties vs. substrate geometry and material in different configurations of substrate holders and its position within the CACVD reactor channel. The uniformity and productivity of diamond-coating process in the industrial reactor having 1-m reaction zone is presented. The coatings were characterized by optical microscopy, scanning electron microscopy (SEM) and Raman spectroscopy.

2. Experimental

2.1. Substrate materials

Different types of carbide tools were employed as substrates in the CACVD diamond-coating deposition processes. For assessment of the coating on flat substrates, indexable carbide inserts made by various suppliers were used: SDCT 09T3 AE FN GH1 (Stellram), SPMA 432W VC2 (Valenite), K313 (Kennametal) and SCMT432-KMH13A (Sandvik). All of these inserts, with the exception of Stellaram, had square geometries (~12×12×3 mm) with and without a central hole. These carbide substrates were installed at near-wall positions using substrate holders as shown in Fig. PI-5a.[1] Cobalt content in these inserts is about 6 wt.%. Most of the coatings were prepared on fine grain Stellram inserts having dimensions of about 8×8 mm. They were installed both at wall positions and suspended in the arc plasma column using a silica cable. For assessment of the diamond coating on substrates having complex geometry, PCB solid carbide drills made by Tycom with diameters ranging from 0.05 to 1 mm were used. Cobalt content in these drills ranges from 12 to 18 wt.%.

Other carbide shank-shape substrates used in this study were solid carbide dental burs having dimensions of about 1.6 mm diameter×19 mm length provided by various suppliers. Cobalt content in the burs ranges from 6 to 8 wt.%. The same geometry was used for metal rod substrates made of 302 stainless steel, tungsten and molybdenum, which can be substituted for carbides in the manufacture of diamond dental burs. Metal rods made of molybdenum and tungsten were prepared with two shapes of the rod's tips, as is required for dental bur applications: hemisphere end and cone end. Rods with cone ends were prepared with cone angles ranging from 5° to 8°.

[1] PI indicates Part I of this paper.

2.2. Substrate predeposition treatment

Predeposition treatment of substrates is a well-known stage of polycrystalline diamond deposition processes designed to provide an increase of diamond nucleation sites and adhesion of diamond coating to the substrate. Different predeposition treatment technologies have been developed to secure diamond coating on substrates made of different materials. In this work, a few pretreatment processes were selected for pretreatment of carbide substrates, stainless steel substrates and substrates made of tungsten or molybdenum.

2.2.1. Predeposition treatment of carbides

A standard procedure [1,15] was taken as a basis for the pretreatment of carbide substrates prior to the CACVD diamond-coating deposition process:

- Etching in 30% HCL/30% HNO_3/H_2O solution to remove cobalt binder from subsurface area.
- Cleaning in an ultrasonic bath with acetone.
- Seeding in submicron diamond slurry in ultrasonic bath to increase the density of diamond nucleation sites.
- Cleaning in acetone.
- Drying by isopropyl alcohol.

Micron-scale diamond media is known to generate a high density of diamond nucleation sites [11,13,23]. During the first phase of this work, the proper etching time to remove cobalt binder from the sub-surface area of the carbide substrate was investigated. The carbide burs (1/16 in. diameter, 3/4 in. long) composed of WC/8 wt.% Co were used as sample substrates for this task. The substrates were divided into three groups: substrates of the first group were subjected to acid etching for 5 min; substrates of the second group, 10 min; and substrates of the third group, 15 min. All other predeposition treatment stages remained unchanged. Several samples of each group were then subjected to plasma processing for 12 h in the CACVD reactor #1 (P=20 Torr, H_2/Ar ratio=15%, transversal power flux=8 W/cm^2), while others were treated for 30 min in a vacuum furnace under an argon/hydrogen atmosphere at 900 °C and 10 Torr.

Reflective optical microscopy and SEM images reveal a severe leaching problem associated with increased etching time. Leaching was not observed on samples having 5 min of etching. However, these samples did not exhibit high-quality continuous diamond film. They exhibited an island-like discontinuous film with diamond-like, "cauliflower-shape" crystals randomly distributed over the tip of the bur. Elemental analysis provided by EDX shows a significant amount of cobalt on the surface of samples, which is known to inhibit diamond nucleation [11].

Samples subjected to 10 min of etching appeared to have had leaching of a few WC crystals on the surface, while after 15 min of etching the WC crystals had practically no

binding: all surface cobalt binder was gone. Carbide bur samples after 10 to 15 min of etching do not exhibit cobalt diffusion to their surfaces when the temperature of the bur tip remains below 900 °C. When the temperature of the bur tip exceeds 950 °C, cobalt diffusion becomes significant even after 15 min of etching. Based upon these results, 10-min cobalt etching was chosen for the predeposition treatment of WC/Co carbide substrates. To eliminate leaching of WC grains, an additional stage of vibratory–abrasion treatment at 60 Hz frequency in a wet B_4C or SiC powder (200 mesh) was introduced after the acid-etching stage to remove leaching WC grains. Optical microscopy analysis provides no evidence of leaching of the WC grains after the vibratory–abrasion treatment.

Different predeposition treatments have been developed for adhesion enhancement of diamond coatings. They include plasma etching, ionitriding, ion implantation and deposition of adhesive sublayers [4,7,19,26–28]. Two ways of such surface treatments of carbide substrates prior to CACVD plasma processing of diamond coatings were used in this work as a substitute for acid etching. First was deposition of diamond-like coatings (DLC) using filtered cathodic arc process [8,9]. Substrate solid carbide burs and PCB drills were coated by carbon DLC to approximately 1 μm thickness followed by loading in the CACVD reactor for deposition of polycrystalline diamond coatings. Second was ionitriding of carbides in CACVD reactor by exposure to nitrogen/hydrogen plasma for 1 h at 800 °C. This was done in a one vacuum cycle with diamond-coating deposition process by creating ionitriding atmosphere in a reactor prior to deposition.

2.2.2. Predeposition treatment of substrates made of molybdenum or tungsten

The predeposition treatment of tungsten and molybdenum substrates is much simpler compared to that of carbide. Their near surface layer carburizes rapidly in hydrocarbon plasma environment providing favorable conditions for subsequent diamond growth [22]. These substrates do not require the acid-etching stage. Alternatively, sandblasting and vibratory tumbling were employed to increase substrate surface roughness. Besides providing mechanical anchoring of diamond films, these treatments are also known to be beneficial for increasing diamond nucleation density [14,22].

2.2.3. Predeposition treatment of stainless steel rod substrates

There are three major obstacles for deposition diamond coatings on ferrous metals [16,17,24]. Two of these are the catalytic effect of black iron growth and thermal expansion mismatches. The third is the high carbon diffusivity under CVD hydrocarbon plasma conditions resulting in deep carburization of the substrate metal [21]. This can pull carbon from the surface preventing against build-up of high-density diamond nucleation sites. Therefore, creating barrier layers and bond coatings can be effective for adhesion control on these types of substrates [7,16,17,26–28]. A multilayer diffusion barrier coating consisting of a TiN layer with a thickness of about 0.5 μm followed by tungsten layer having a thickness of about 2 μm was deposited on stainless steel rod substrates using large area filtered arc deposition (LAFAD) technology [9]. Surface roughening by sandblasting and vibratory tumbling was used for stainless steel (SS) substrate rods prior to deposition of the LAFAD PVD bond coating.

After the deposition of the TiN/W coating, the stainless steel rod substrates were subjected to the diamond microabrasion seeding process identical to that used for the substrates made of carbide, tungsten and molybdenum.

2.3. Deposition of diamond coatings

For preparation of the diamond coatings, the substrates to be coated were positioned both on the substrate holders installed through the wall of the reaction channel or suspended in the arc plasma column along the axis of the reactor as previously described in Figs. PI-4 and PI-5 of this paper. The characteristic parameters of the diamond-coating deposition process are presented in Table 1. Table 2 presents the typical settings for various process stages of the deposition of diamond coatings on carbide substrates. The process started from the decarburisation stage, which lasted for 10 min. At this stage, substrate temperature was maintained at approximately 850 °C in argon/20% hydrogen plasma. This stage was followed by 10 min of accelerated carbon nucleating stage when up to 1.5 % methane composed the plasma environment. These two consecutive stages were found to be beneficial for increasing the density of diamond nucleation sites on carbides and other substrates [10,19,22]. The regular nucleation stage followed and lasted about 40 min with the methane concentration reduced to 0.3% while the substrate temperature was maintained at 850 °C. This was

Table 1
Characteristic parameters of CACVD processing of polycrystalline diamond coatings

Item	Parameter	Unit	Value
1	Pressure	Torr	3–50
2	Ar flow rate	slm	0.5–5
3	H_2 concentration in Ar	%	10–50
4	CH_4 concentration in H_2	%	0.4–2
5	Side energy flow P_s	W/cm^2	3.5–60
6	Volume density of power P_c	W/ cm^3	5–80
7	Electric field E_a in an arc column	V/cm	1–6
8	Arc current	A	12–32 in reactor #1; 50–70 in reactor #2
9	Inside diameter of reactor channel	cm	3.0 in reactor #1; 4.0 in reactor #2
10	Length of reaction zone	cm	100

Table 2
Typical process settings during various process stages for carbide substrates

Stage	P (Torr)	H_2/Ar (%)	CH_4/H_2 (%)	V_{arc} (E, V/cm)	I_{arc} (A)	Transversal power flux (W/cm^2)	Specific volume power (W/cm^3)	Time (min)
1. Decarburisation	20	10	0	180	24			10
2. Accelerated nucleating	20	10	1.5	170 (2.9)	26	7.9	10.7	10
3. Nucleating	20	15	0.03	165	26			40
4. High-temperature deposition	20	15	0.03–0.06	170 (2.9)	26	7.9	10.7	60–120
5. Low-temperature deposition	20	7	0.03–0.06	150	24	5.0	7.5	120–180

followed by the high-temperature diamond deposition stage during which the substrate temperature was reduced to 800 °C, and methane concentration ranged from 0.3% to 0.6% followed by a low-temperature deposition stage when substrate temperature was reduced to 650–700 °C. Substrate temperature reduction was aimed at relieving thermal stresses in the coating [29]. The duration of the last deposition stage was varied depending upon the desired thickness of the coating.

2.4. Diamond film analysis

The coating morphology was characterized by reflecting optical microscopy and SEM. In some cases, electron backscattering and EDX were used for analysis of surface composition. SEM analysis for the majority of the samples was performed at the facilities of the metallurgical laboratory of the Material Science department of the University of Toronto.

The quality of the diamond coatings was investigated by Raman spectroscopy at Photonics Research Ontario (PRO) facilities at the University of Toronto. Crystalline diamond yields a very sharp and strong Raman peak at 1332 cm^{-1} [25]. Crystalline graphite displays a sharp peak at 1580 cm^{-1}, while highly polycrystalline graphitic carbon shows very broad peaks at 1575 and ~1350 cm^{-1}. There is a smooth transition between the spectra for polycrystalline graphite and amorphous carbon, making it difficult to judge the relative character of each form of carbon in the film when these two peaks are observed.

The spectra were collected using a JY-Horiba LabRam microRaman system with a 514.5-nm argon ion laser for excitation. The samples were mounted on a standard microscope stage adapted to bring the light incident on the film in a well-defined 1-μm-diameter spot and collect the backscattering light. A single-grating spectrometer equipped with a CCD array detector records the spectrum.

Typical conditions were 200 mW of laser power at the source (~80 mW at the sample) and collection times of 0.25 s averaged five times for each spectrum. In the case of substrate metal rods, a total of five spectra were recorded from the tip of each rod, with one spectrum collected from the center region and four spectra collected from roughly equally spaced regions closer to the edge of the tip. The five spectra were then averaged together to produce an average spectrum for the rod tip.

3. Results and discussion

3.1. Diamond film properties

3.1.1. CACVD diamond coating of carbide inserts

All experiments were conducted in reactor #1. SDCT 09T3 AE FN GH1 (Stellram) indexable carbide inserts were suspended on a silica cable in the arc column creating a chain along the axis of the reactor channel. Each of the inserts in the chain was separated from the neighbor insert by a 2-mm-thick ceramic spacer. The substrate inserts were rotating at 4 rpm by rotating the silica cable. For further equalization of plasma parameters across the reaction channel, the direction of the rotational magnetic field was alternated each 5 min. In addition, the direction of the gas vortex was also alternated each 10 min by switching the gas injecting channels. In this case, the temperature of the substrate is determined by the balance between the thermal flux conveyed by plasma and radiation cooling as depicted in Figs. PI-12 and PI-13. Fig. PII-1 shows a typical SEM image of the diamond film deposited in these conditions. It can be seen that the diamond film divides into separate crystals at the face surface of the insert while at the side surface it appears to be a continuous coating with uniform distribution of diamond grains. This can be attributed to the screening effect of neighbor inserts in the chain. The uniform distribution of diamond crystals both on the side and face surfaces of the insert was achieved by increasing the distance between inserts in the chain to 4 mm using two ceramic spacers. The photograph of the diamond crystals as well as Raman spectra from the spot near the corner of the insert demonstrates that high quality of diamond coating can be achieved in this arrangement (Fig. PII-2). It was found that in case of freestanding substrates, cooling only by thermal radiation, the optimization of the plasma parameters became easier in reactor #2, having a larger channel diameter.

Using wall-through substrate holders shown in Fig. PI-6a with CPVCI thermal regulating layer disposed between

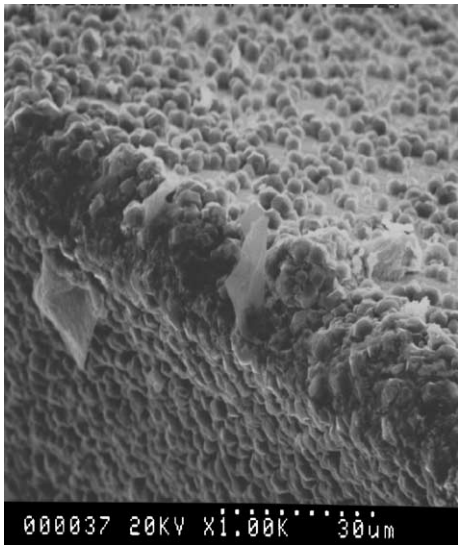

Fig. PII-1. Diamond coating deposited on carbide insert suspended in the arc plasma column, 2-mm distance between neighbor inserts in a chain (see Fig. PI-4a).

substrate insert and substrate holder mount makes thermal management of inserts much more precise in CACVD processes. In this case, continuous diamond film forms over the entire insert area exposed in plasma (Fig. PII-3a). XRD spectra reveal the [111] peak of the diamond coating on the surface of insert (Fig. PII-3b). An SEM image of the diamond coating on a face surface of the insert near its center is shown in Fig. PII-3c. The size of diamond crystals is slightly greater on the edge of the insert, which can be attributed to higher temperature at the edges (Fig. PII-3d). The thickness of the film was controlled by deposition time with other process parameters such as pressure and transversal power flow held constant. Thickness distribution vs. processing time for the diamond coatings deposited on Kennametal K313 carbide inserts in different process runs is shown in Fig. PII-3e. All of these coatings were deposited at 20 Torr with approximately 10 W/cm^2 transversal power flow and CH_4/H_2 ratio=0.6%. The figure shows that for this set of process parameters the deposition rate ranges from 1 to 2 μm/h. Consider the ratio:

$$\gamma \sim \frac{h_{\text{face}}}{h_{\text{corner}}},$$

where h_{face} and h_{corner} are the thicknesses of the diamond coating on the face side and corner of the inserts, respectively. Build-up of coating thickness on edges was observed on substrate inserts installed without active thermal management, which results in a substantial temperature difference between bulk and edge regions [15]. It can be seen that γ ranges from 30% to 60% at small deposition time and increases to near 90% when deposition time increases.

3.1.2. CACVD diamond coating of shank-shape carbide substrates

All coatings presented in this subsection were deposited in reactor #1 with typical process parameters presented in Table 2. Carbide drills and burs were used as substrates for investigating the influence of process parameters on diamond-coating phase composition and morphology. The influence of predeposition treatment on the morphology of

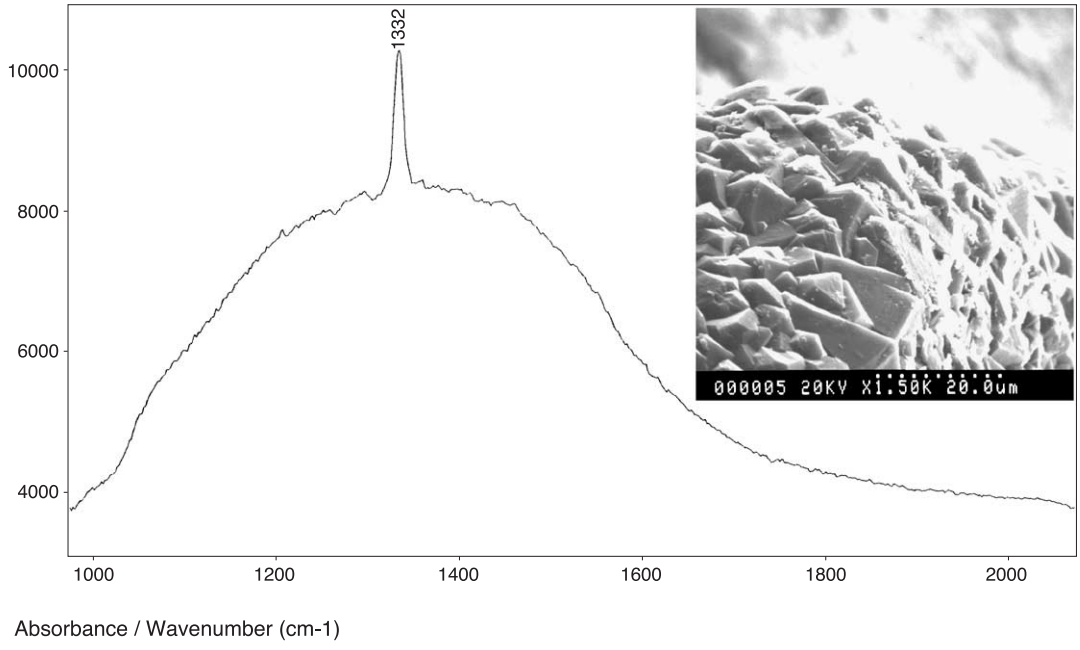

Fig. PII-2. Raman spectra and SEM image of diamond coating deposited on carbide insert suspended in the arc plasma column, 4-mm distance between neighbor inserts in a chain (see Fig. PI-4a).

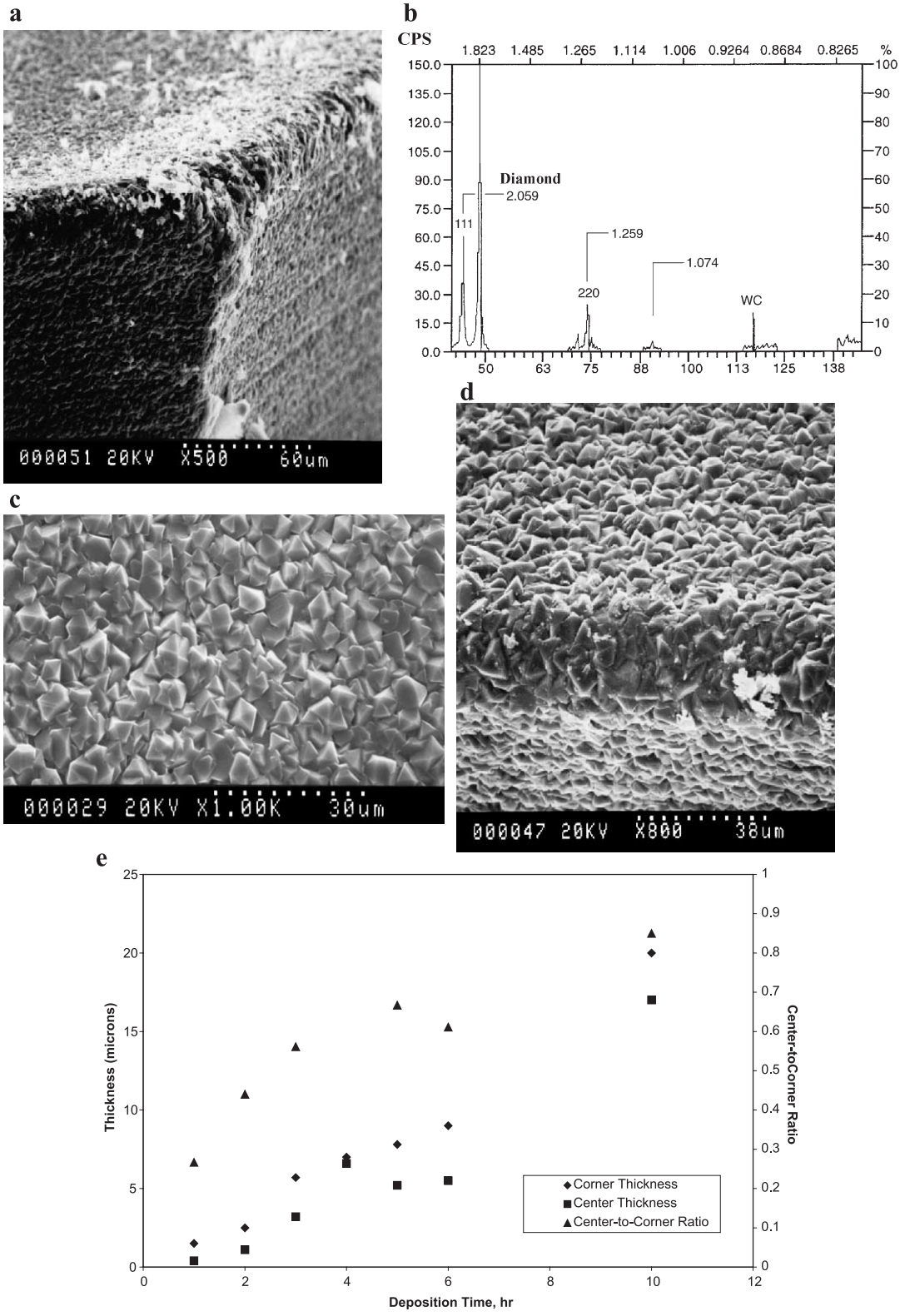

Fig. PII-3. (a) Diamond coating on carbide insert installed at the wall of the CACVD reactor using the substrate holder shown in Figs. PI-5 and PI-6a. (b) XRD spectra of diamond coating taken from the face side of the carbide insert. (c) SEM image of diamond coating on the face side of the carbide insert. (d) SEM image of diamond coating on the cutting edge of the carbide insert. (e). Thickness of diamond coatings deposited on carbide inserts in different process runs vs. deposition time.

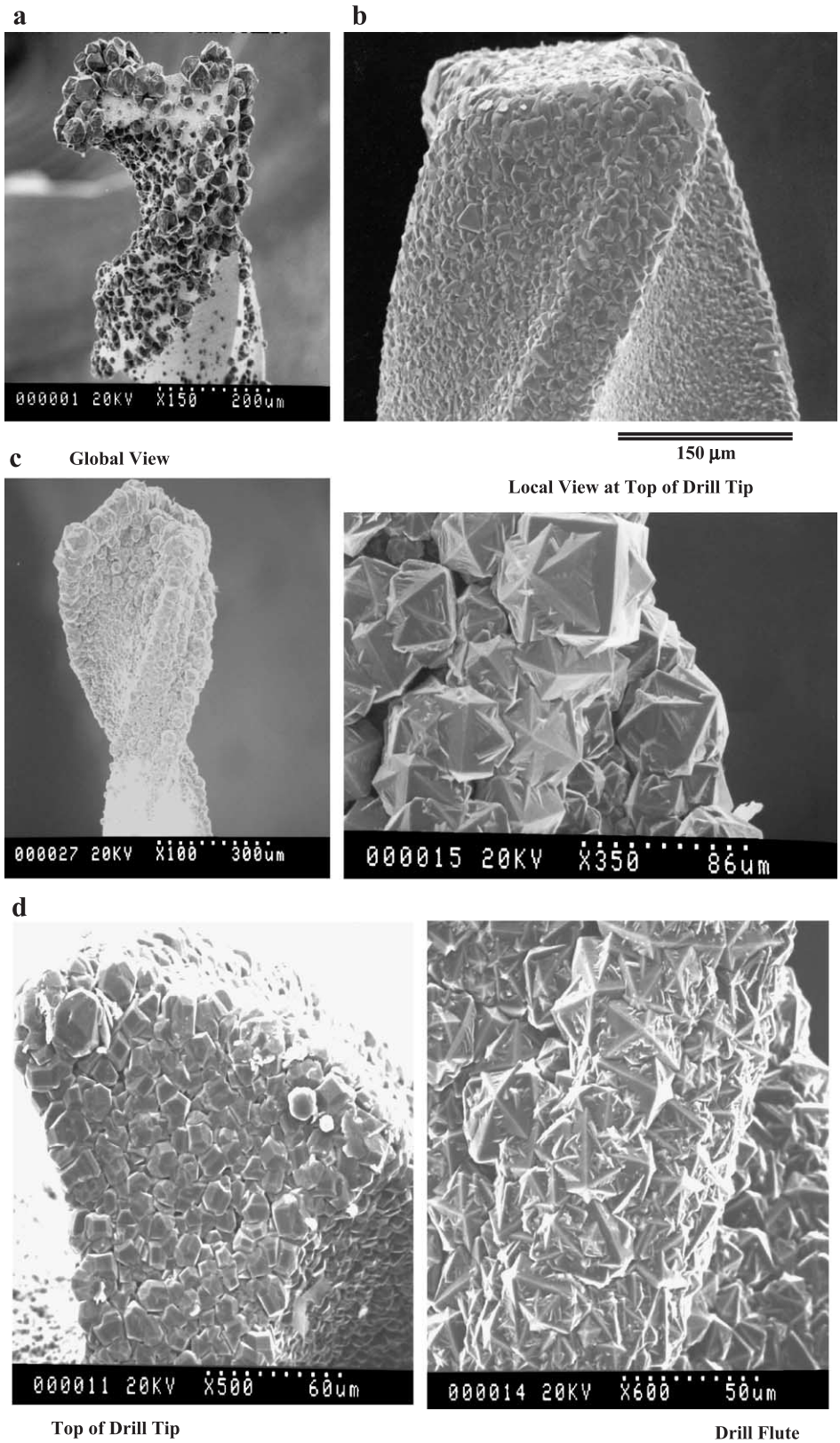

Fig. PII-4. (a) Diamond coating on carbide drill substrate subjected to 10 min of micro-abrasion in submicron diamond slurry. (b). Diamond coating on carbide drill substrate subjected to 1 h of micro-abrasion in submicron diamond slurry. (c). Diamond coating on carbide drill substrate with filtered arc DLC bond layer (not subjected to micro-abrasion). (d). Diamond coating on carbide drill with N_2/H_2 plasma ionitriding pretreatment at 800 °C.

the diamond films deposited on shank-shape carbide substrates is demonstrated in Fig. PII-4a–d. Besides predeposition treatments, all diamond-coating deposition parameters were identical to those outlined in Section 2.3. Comparison of these coatings demonstrates the influence of predeposition treatment on the morphology of diamond coatings in the CACVD process. Pre-scratched carbide substrates have fine diamond coatings with grains 10–20 times less than unscratched carbide substrates with DLC sublayer as has been reported elsewhere [1,11,13,15,23]. The deposition rate of fine coating (Fig. PII-4b) is about 2–3 μm/h, while for coarse coating (Fig. PII-4a,c) the large diamond crystals grow with a rate of about 10 to 15 μm/h. The larger crystals are located at the edge of the flute, which can be attributed to higher temperature in this area of substrate [15]. Secondary diamond nucleation and appearance of multiply twinned diamond crystals can be observed on the drill flute near the top of the drill tip, which can also be attributed to intense electron bombardment during CACVD diamond deposition process, similar to that reported in Ref. [30]. It can be seen that ionitriding promotes continuous diamond film growth on carbides without necessitating the cobalt etching stage. However, the drawback of both DLC bond sublayer and ionitriding approach is the relatively low density of diamond nucleation sites as was also found in Refs. [4,27]. This results in surface morphology similar to that displayed in Fig. PII-4c, which has a relatively low concentration of large diamond crystals. It also shows secondary diamond nucleation along the drill flute.

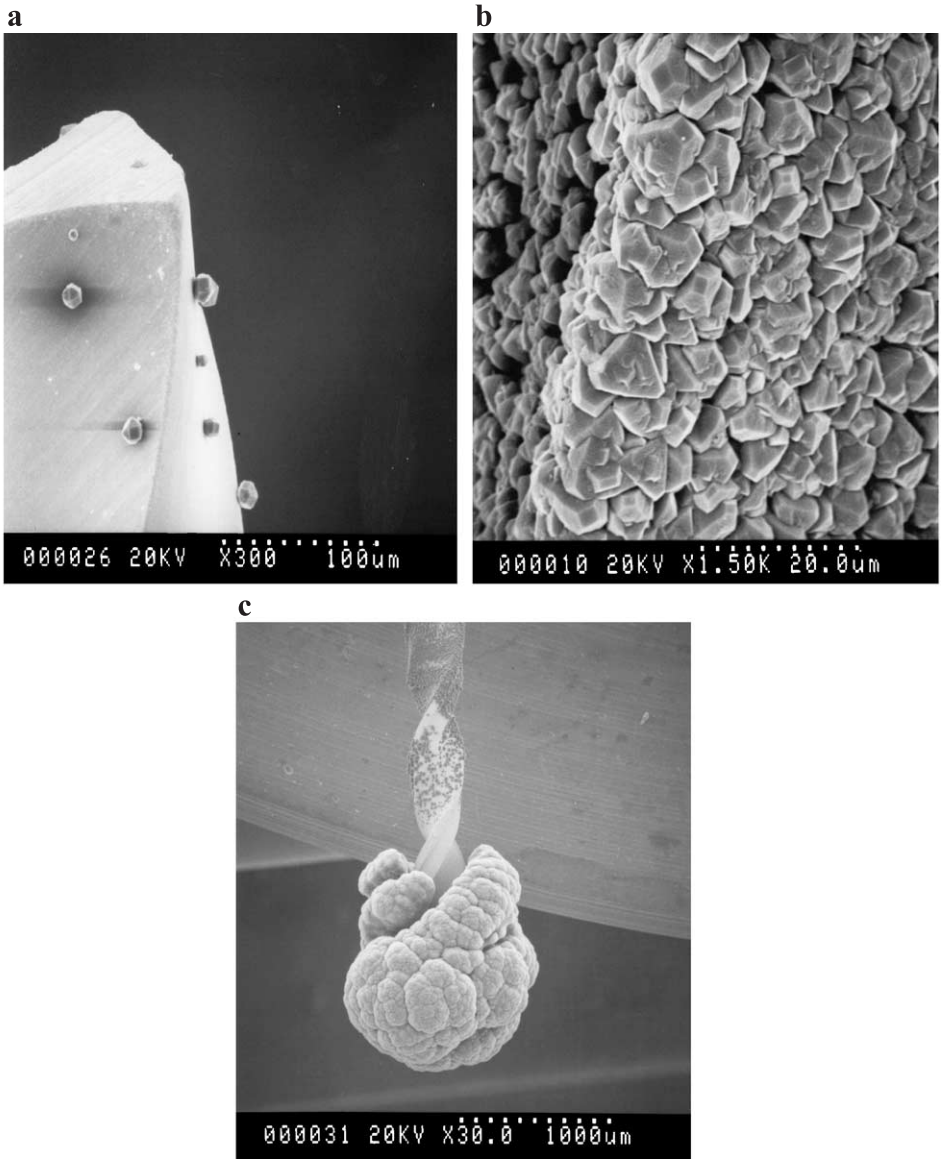

Fig. PII-5. (a) Diamond coating on carbide drill substrate installed in the opening of the substrate holder flush with substrate holder mount surface. (b) Diamond coating on carbide drill substrate installed in the opening of the substrate holder projected 3 mm toward the reactor's axes. (c) Carbon coating on carbide drill substrate installed in the opening of the substrate holder projected 8 mm toward the reactor's axes.

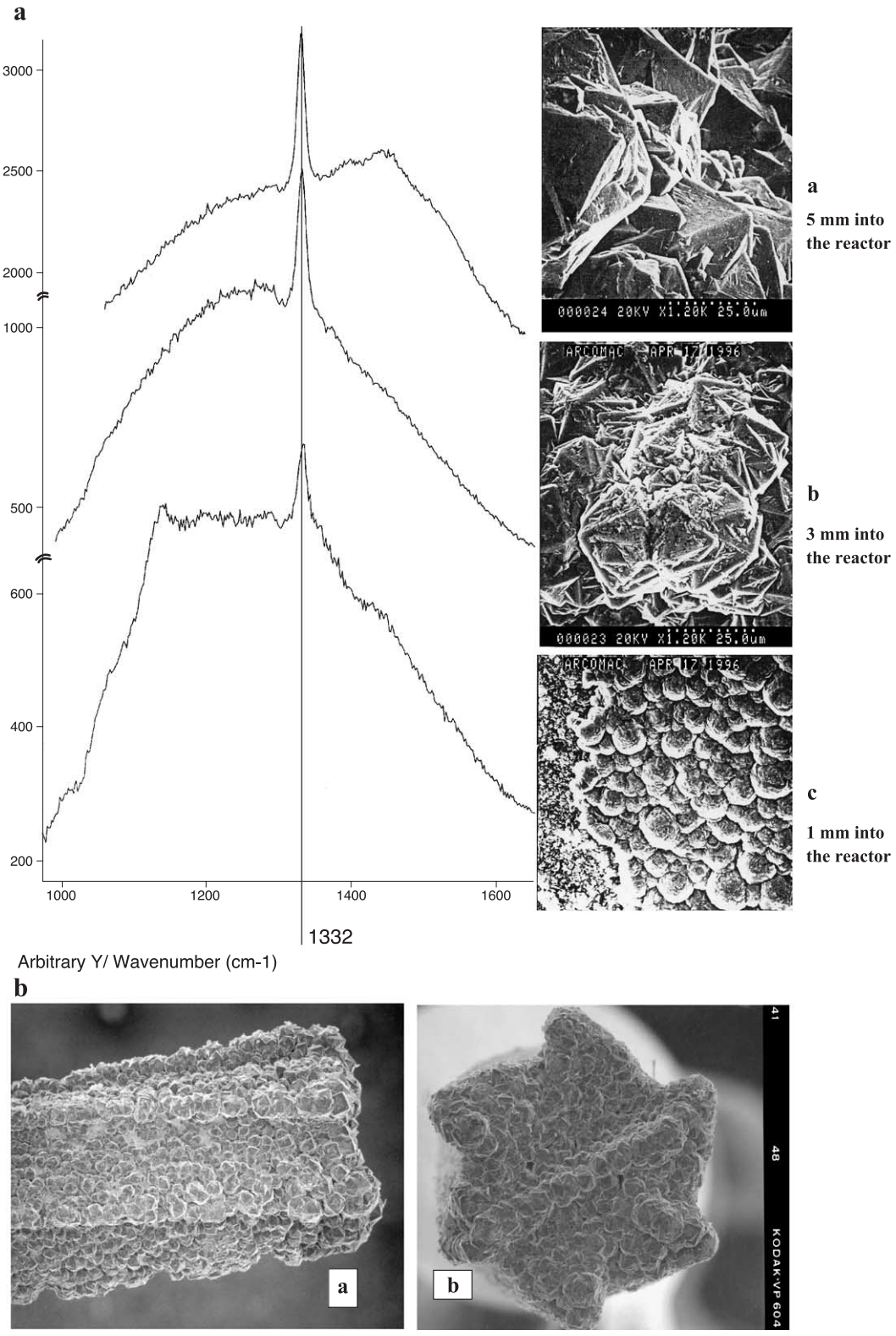

Fig. PII-6. (a) SEM images and corresponding Raman spectra of diamond coating taken from three spots along the carbide bur's flute (1.6 mm diameter) with the first spot at the very tip of the bur (first spot, projected 5 mm toward the reactor's axes; second spot, 3 mm; third spot, 1 mm). Ratio CH_4/H_2=1.5%. Courtesy of Dr. X. Go (Photonics Research Ontario, Toronto, Canada). (b) SEM images of diamond coating on carbide bur projected 5 mm toward the reactor's axes. Ratio CH_4/H_2=0.6%.

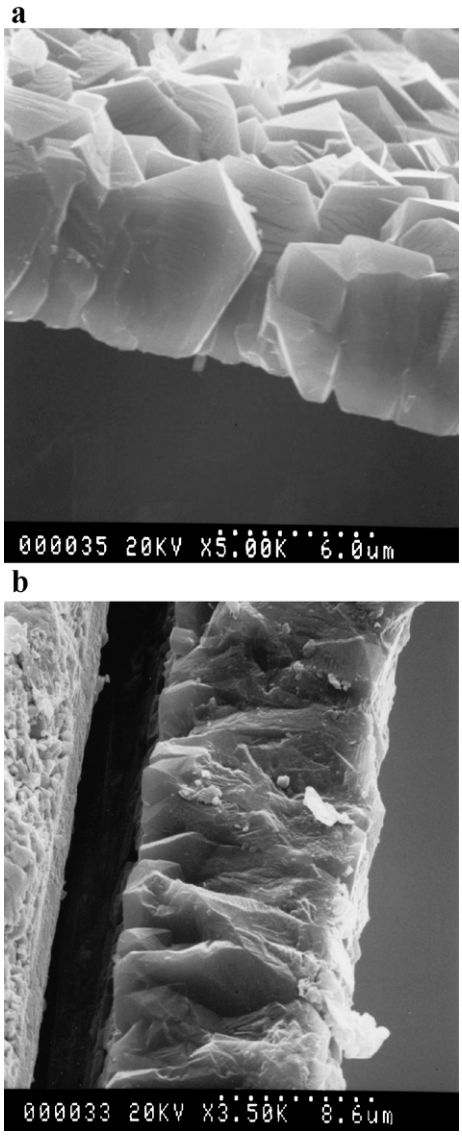

Fig. PII-7. Free standing diamond films deposited on carbide substrate with different H_2/Ar ratio: (a) ratio H_2/Ar=10%; (b) ratio H_2/Ar=15%.

Fig. PII-5 illustrates the influence of substrate position, relative to the arc column, on diamond-coating morphology. The process parameters and type of carbide drill substrates were the same as in the process presented in Fig. PII-4. Fig. PII-5a shows a carbide microdrill which was installed in the opening of the substrate holder flush with the substrate holder surface. In this case, the diamond film appeared to be noncontinuous, having separated well-faceted diamond crystals with sizes up to 30–40 μm and characteristic distance between neighboring crystals of about 60 μm at the tip of the drill. The growth rate of diamond crystals ranges from 3 to 5 μm/h. In the same process, other microdrills were installed shifted toward the reactor axis in such a way that the top of their tips were projected 4 mm (Fig. PII-5b) and 8 mm (Fig. PII-5c) above the substrate holder surface. This positioned the tips of these drills to be immersed in the arc plasma column at different distances from the reactor axis. The drill flute shown in Fig. PII-5b exhibits a continuous diamond film with a well-faceted polycrystalline structure deposited at a rate of about 5 μm/h. Conversely, the tip of the drill shown in Fig. PII-5c exhibits a 1-mm-diameter graphite ball which had formed with a growth rate of up to 200 μm/h during the same (5 h) deposition process.

Two factors greatly influence the crystal growth shown in Fig. PII-5. First is the temperature of the substrate surface and second is the diffusion flux of precursors conveyed by plasma toward the substrate. Both of these factors are extremely sensitive in the area of the substrate that is immersed in plasma. In the case shown in Fig. PII-5c, an exponential increase of the deposition rate of the carbon layer can be seen in the vicinity of the overheated part of the drill tip, while below the graphite ball, well-faceted polycrystalline diamond coating with a deposition rate of about 5 to 10 μm/h can be observed. This can be explained by nonlinear heat transfer along the drill flute from the tip of the drill receiving energy flux from the surrounding arc plasma toward the cooled part of the drill disposed in the openings of the substrate holder. In this case, the temperature of the overheated spot in the vicinity of the top point of the drill tip is determined by the balance between the energy flux from plasma and radiative losses. When the diameter of substrate drills is less than 0.5 mm, a dramatic increase in the thermal gradient along the drill tip exposed in plasma results. In this case, the temperature of the tip is primarily determined by the balance between the thermal flux conveyed by plasma and radiation cooling similar to the case shown in Fig. PI-15a.

Fig. PII-6a shows three SEM images and corresponding Raman spectra taken from three points along the tip of a 2-mm-diameter×19-mm-long carbide bur which was extended into the reactor channel 5 mm. The process

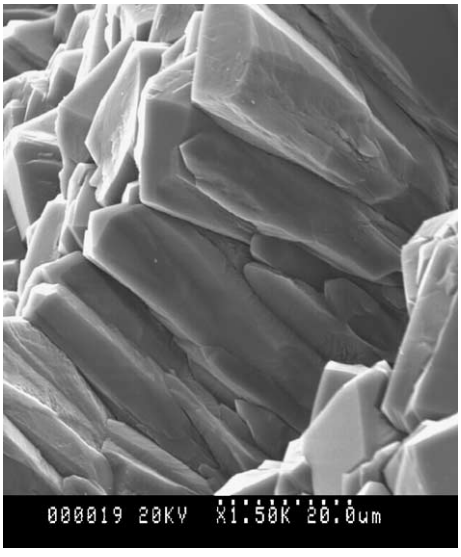

Fig. PII-8. SEM image of diamond coating near the crack of tungsten rod substrate.

settings for this coating run were unchanged from the coatings shown in Figs. PII-4 and PII-5 with the exception of the methane-to-hydrogen ratio, which was increased in this case to 1.5%. The first point was taken from the top of the tip (5 mm into the channel), the second from the middle (~3 mm into the channel) and the third from the bottom (~1 mm into the channel). In this case, the sizes of diamond crystals diminish along the flute from the top point of the bur's tip toward the bottom. The morphology of the diamond crystals also degrades in the same direction of decreasing substrate temperature similar to that observed in similar conditions of hollow cathode are assisted CVD diamond synthesis process [30]. Similar results were found for diamond coatings on cylindrical geometries in Ref. [18]. It was also observed from arc jet assisted CVD diamond-coating deposition process that the concentration of amorphous carbon increases when the distance from the arc torch nozzle increases [22]. Fig. PII-6b shows an SEM image of a bur of the same geometry, but having a larger diameter (~1.6 mm) installed in the same position in the same reactor. It was processed with identical process settings as for the bur shown in Fig. PII-6a, but in this case the methane-to-hydrogen ratio was set at 0.6%. It can be seen that, in this case, the distribution of diamond crystals along the shank of the bur demonstrates a high degree of uniformity. The Raman spectra taken from the tip butt-end and from a point located at 1 mm into the reactor channel do not show significant differences.

Fig. PII-7 shows the difference in the deposition rates when the hydrogen-to-argon ratio increases, while other process parameters remain unchanged. It can be seen that the film thickness in Fig. PII-7b is approximately two

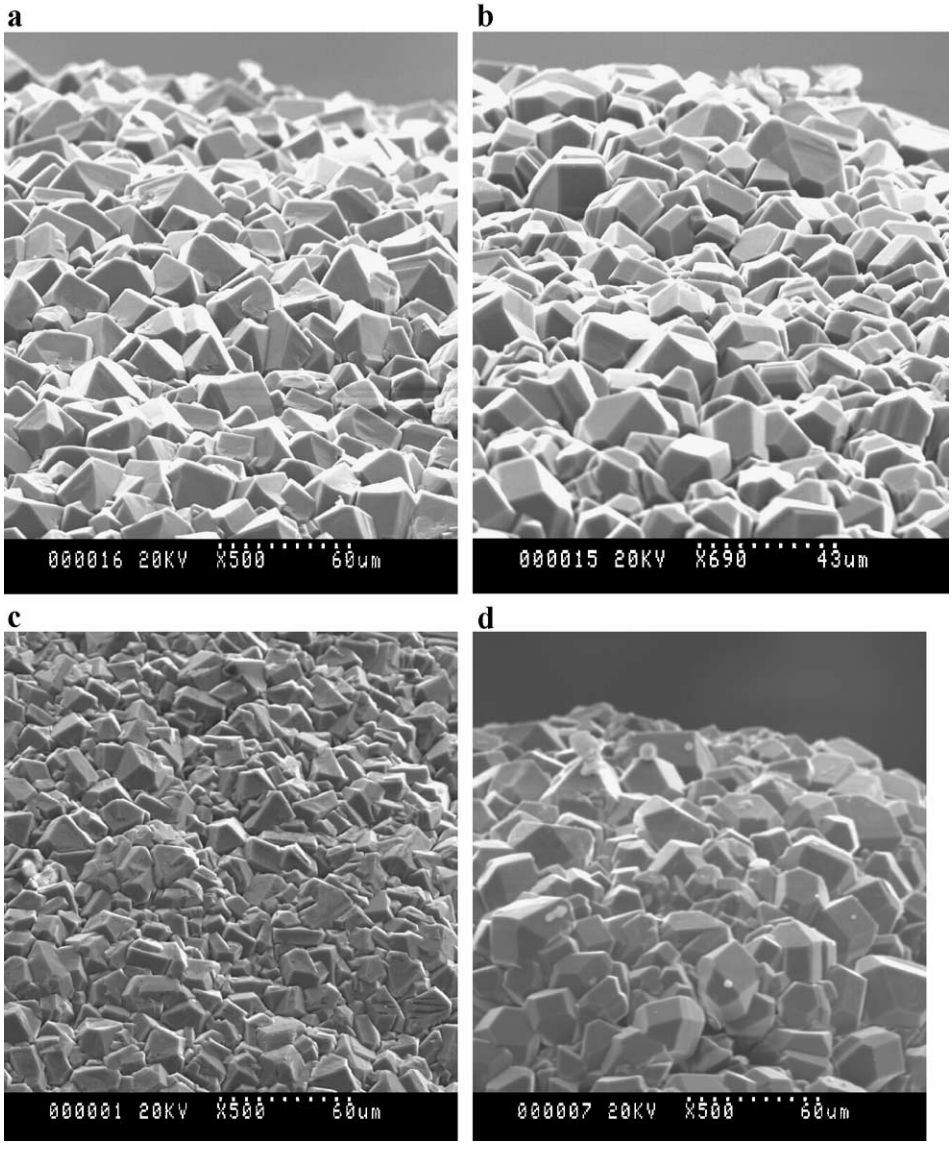

Fig. PII-9. SEM images of diamond coating deposited on the very tip of metal rod substrates subjected to roughening by sand blasting: (a,b) tungsten rod substrate; (c,d) molybdenum rod substrate.

times that of the film thickness shown in Fig. PII-7a. The increase in deposition rate is attributed to the 30% increase of the hydrogen-to-argon ratio and associated increase of the transversal power flux similar to the influence of total pressure increase [12].

3.2. Productivity and uniformity of diamond-coating deposition in industrial-scale CACVD process

Assessment of the diamond coatings prepared in a fully loaded CACVD reactor process run vs. substrate material and position of shank-shape substrates in the reactor was performed in reactor #2. Tungsten and molybdenum rods as well as stainless steel rods having a geometry similar to conventional dental burs were used as substrates in this run. The total number of substrates installed along the wall of the reactor channel was about 700, which completed 10 sections of the reactor, while the total capacity of reactor #2 is more than 1000 metal rods per 15 reactor sections. Typical process parameters were the following: pressure, 7 Torr; H_2/Ar, ~20%; CH_4/H_2, ~0.6%; arc current, 65 A; arc electric field, ~2.5 V/cm; and transversal energy flow, ~13 W/cm^2. Both longitudinal and transversal (rotational) magnetic fields were used in this process. The duration of the run was 20 h. The metal rod substrates were mounted at the wall-through substrate holders as shown schematically in Fig. PI-6b.

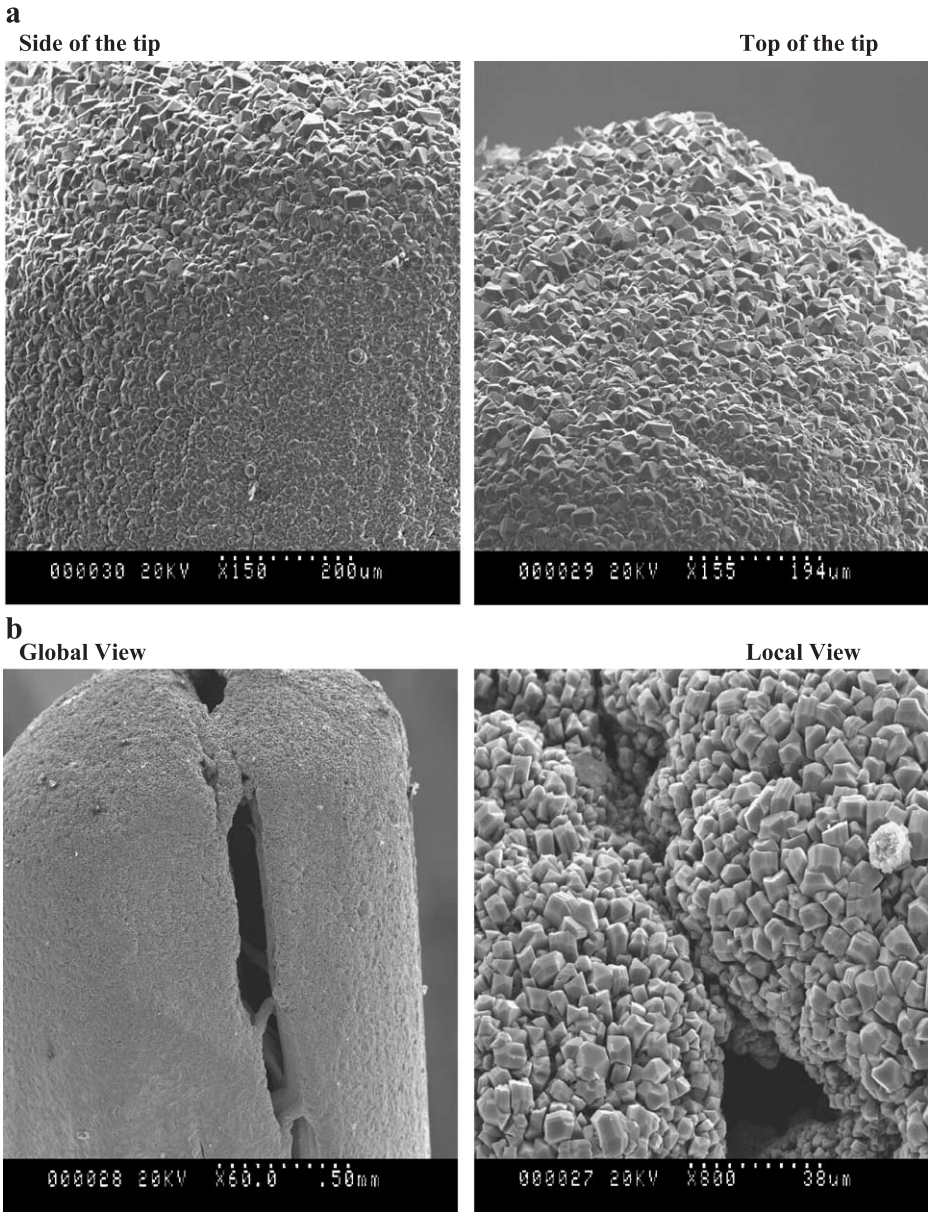

Fig. PII-10. (a) Surface patterns of diamond coating on tungsten rod subjected to sandblasting roughening pretreatment. (b) Conformal diamond coating of molybdenum rod having mechanical crack.

3.2.1. CACVD diamond-coating morphology on metal rod substrates

Fig. PII-8 shows the side view of the diamond coating responding to a mechanical crack on a tungsten rod substrate. It can be seen that diamond crystals exhibit a columnar morphology with a height of about 60–70 μm and width at the substrate interface of about 10 μm. These columnar crystals exhibit cubic, octahedral and cubo-octahedral geometries. The thickness of the coating can be estimated by the height of the diamond crystals. This estimation yields a thickness in the range of 60–70 μm for coatings deposited on tungsten rods. Based upon this estimation, the rate of deposition for a 20-h process is calculated to be 3–3.5 μm/h. Comparison of coatings deposited on tungsten and molybdenum rods shows that the characteristic diamond crystal size on molybdenum rod tips is about 1.5 times larger than those deposited on tungsten. The rate of deposition of diamond coating on molybdenum substrates is also slightly higher than for tungsten: 4–4.5 μm/h. This can be attributed to the differences in initial substrate surface morphology: the tungsten burs have a smooth uniform surface, while the molybdenum burs have large lamination cracks. Generally, diamond coatings on both tungsten and molybdenum substrates appear to have well-shaped crystals, often exhibiting significant secondary nucleation. Crystal sizes diminish slightly from the tip down. The habitus of the crystals is changing in the same direction, with increasing cube concentration oriented parallel to the surface. Diamond coating on molybdenum rods exhibits few cubes and more prisms than that on tungsten. Qualitative comparison of coatings presented in Fig. PII-9 reveals that diamond coating on tungsten is composed of almost entirely well-faceted cubical and octahedral shapes, while on molybdenum rod tips, a significant portion of crystals have intermediate shapes. Surface patterns both on molybdenum and tungsten burs exhibit hills and valleys created by the sandblasting pretreatment stage as illus-

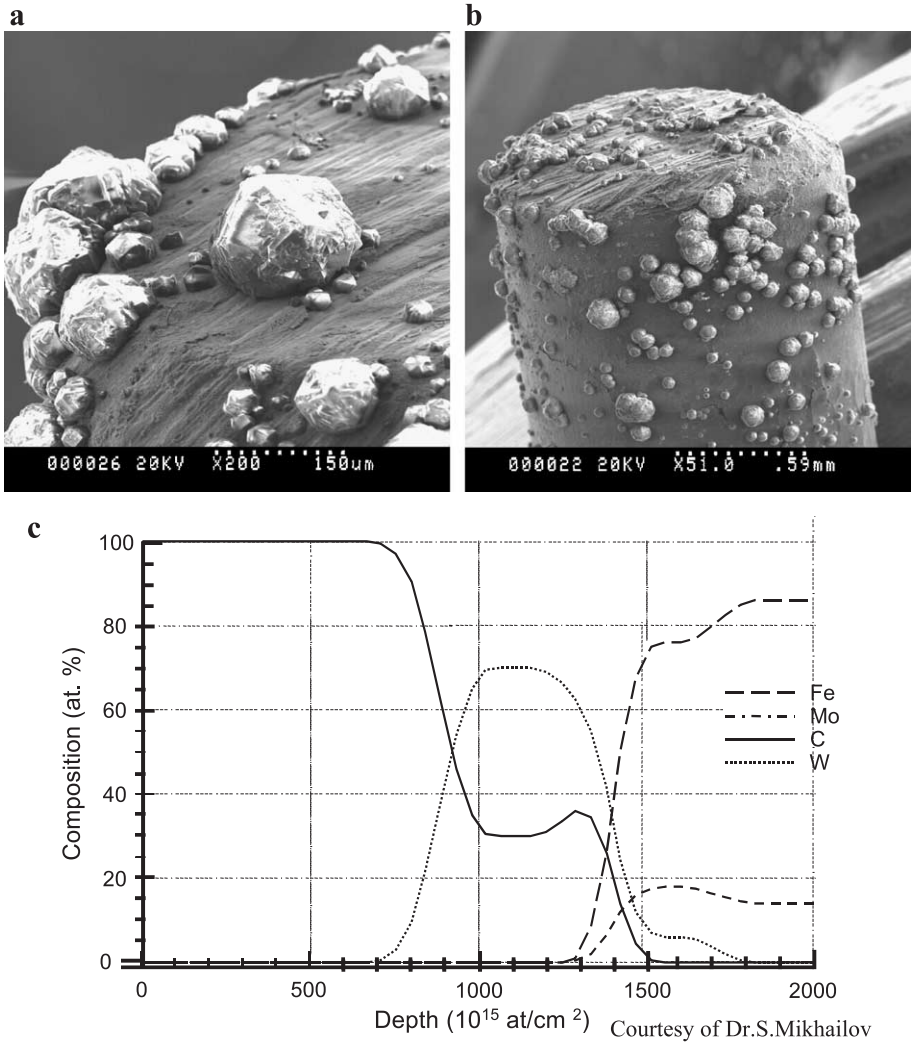

Fig. PII-11. Diamond coating on the tip of stainless steel rod (1.6 mm diameter) with filtered arc TiN/W bond layer. (a) very tip; (b) top shank; (c) RBS spectrum. (Courtesy of Dr. S. Mikhailov.)

trated in Fig. PII-10a. Substrate cracks occasionally appear, predominantly on the molybdenum substrate burs as a result of the mechanical manufacturing process. It can be seen in Fig. PII-10b that the diamond crystals penetrate deeply into the crack's gap, coating both sides of the crack uniformly. This demonstrates that in the CACVD process, diamond coating can be deposited on well-roughened surfaces without sacrificing coating integrity, which can dramatically increase coating adhesion.

Fig. PII-11 shows SEM images of stainless steel rod substrates subjected to the same CACVD process together with molybdenum and tungsten rods. The steel substrate rods were pre-coated with a TiN/W barrier layer as explained in Section 2.2. Ionitriding of stainless steel substrates under the PVD sublayer was also applied to selected samples creating a multilayer architecture similar to that reported in Refs. [7,8,27]. A sample of the RBS spectra of carbon coating deposited on stainless steel over tungsten barrier sublayer is shown in Fig. PII-11c. It can be seen from Fig. PII-11a,b that the coating does not appear to be continuous, but rather consists of single crystals or groups of crystals randomly distributed over the top and side surfaces in the vicinity of the front butt-ends of the stainless steel rods. Most of the crystals show almost perfect diamond morphology, while some of them develop into intermediate shapes between well-faceted diamonds and cauliflower-like shapes, as a result of intensive secondary nucleation. Fig. PII-11 also shows a variety of sizes among diamond crystals both on the top and side surfaces of the rods. Some of the crystals grow up to 250 μm, while the average size of larger crystals is estimated at 100 μm. Among the larger crystals there is an abundance of smaller crystals with characteristic sizes ranging from 20 to 40 μm. The discontinuity of the diamond coating on the stainless steel rods in this experiment may be attributed to the insufficient thickness of the TiN/W barrier layer which permits carbon interdiffusion into the stainless steel substrate. This reduces the effect of submicron diamond abrasion and results in a low density of diamond nucleation sites. Another factor that has critical influence on diamond-coating morphology is substrate temperature. During the process, the temperature of stainless steel rods is much higher than that of carbide, tungsten, or molybdenum rods due to the significant difference in the thermal conductivity of these materials. The thermal conductivity of tungsten is approximately 1.2 W/m K, while that of

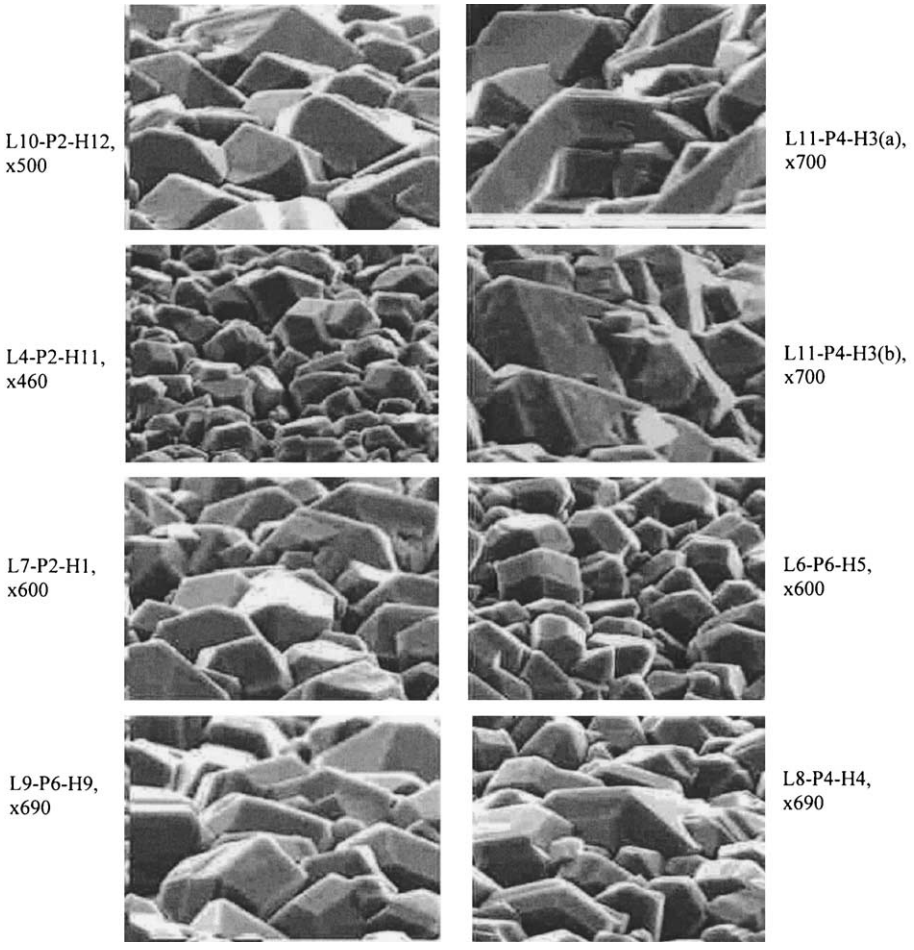

Fig. PII-12. Diamond coatings on molybdenum rods installed in randomly distributed positions throughout the reactor channel.

stainless steel ranges from 0.1 to 0.2 W/m K near the 1000 °C typical substrate temperature. Inspection of the stainless steel rods revealed that some were beginning to melt, indicating that the characteristic temperature of the rod tips ranges from 1200 to 1300 °C. This can induce graphitisation of synthetic diamond crystals. It was found that even on the melted tip surface a group of large, diamond-like crystals were deposited.

3.2.2. Diamond-coating quality vs. substrate material and position within the reactor

Figs. PII-12 and PII-13 show SEM images of diamond coatings deposited on molybdenum and tungsten rods mounted in randomly distributed positions throughout the reactor. From this, it can be inferred that there is no relationship between coating morphology and substrate position within the reactor. Differences in the size of crystals do not correlate with position in the reaction zone, at least for reactor sections #5 through #13, but rather with initial surface profile of the tips and with differences in predeposition treatment. It was found that upstream sections located close to the cathode generate larger crystals. The presence of arc plasma instabilities and nonuniformity of reaction species distribution in the area at the entrance of the reaction zone may explain this phenomenon. This can result in more intensive energy and mass transfer resulting in the growth of larger crystals.

The following analysis of coating uniformity vs. substrate material and position within the reaction zone was performed in Photonics Research Ontario by micro-Raman spectroscopy.

3.3. W Substrate

First, a series of 11 tungsten rods processed in the same 20-h run as previously described were selected for sampling from randomly distributed positions throughout the reactor. In Fig. PII-14, the normalized spectrum is presented so that the spectral shapes can be compared. It can be seen that a rather wide range of intensities is observed: both the absolute intensities of the fluorescent component and the intensities of the sharp diamond peak at 1332 cm^{-1}. However, it is worth noting that similarly striking differences in intensities were also observed between the spectra from the same rod tip, indicating that the thickness of the film and/or the local morphology of the film play a role in the spectral intensity.

In general terms, the spectra are quite similar, all displaying a diamond peak with an underlying fluores-

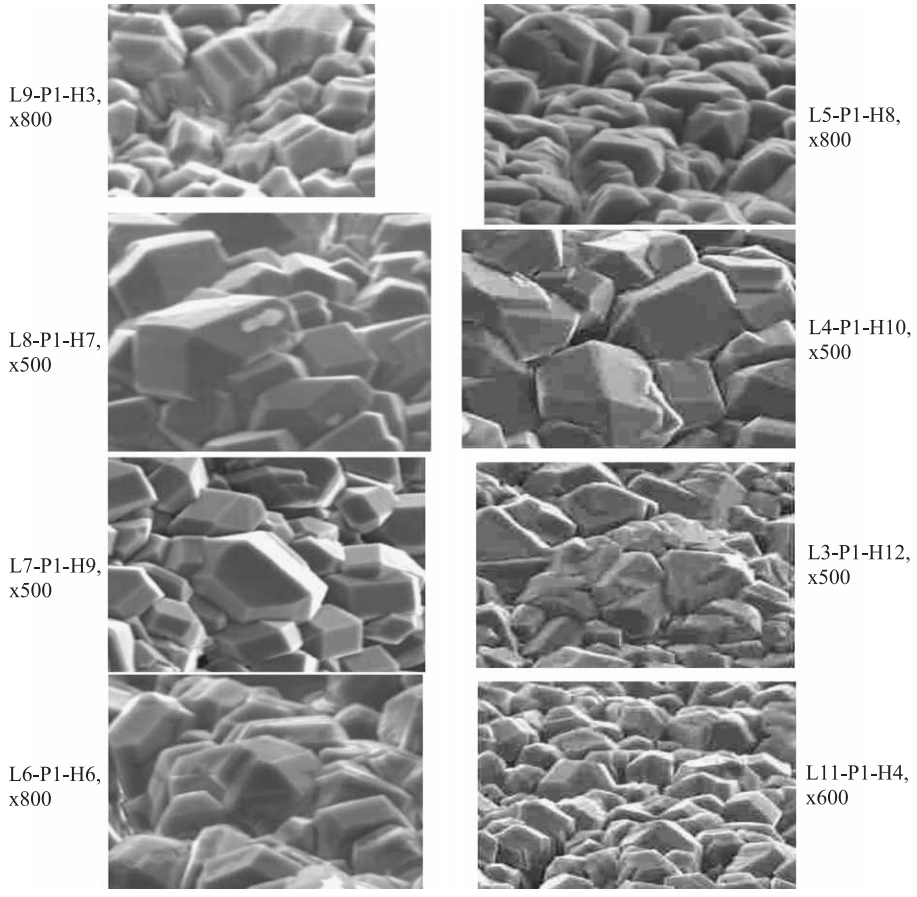

Fig. PII-13. Diamond coatings on tungsten rods installed in randomly distributed positions throughout the reactor channel (same run as in Fig. PII-12).

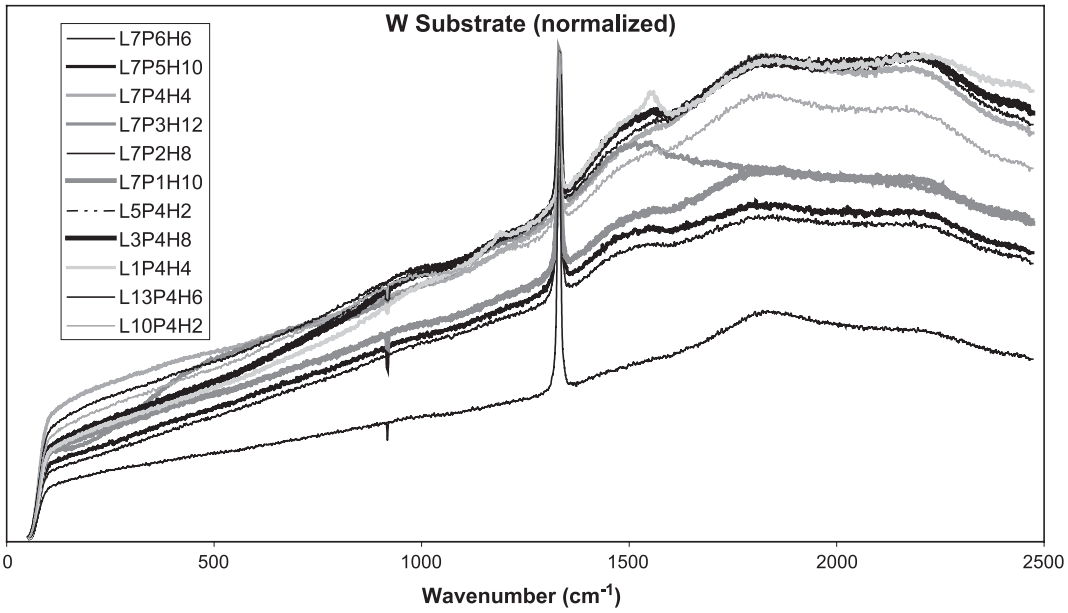

Fig. PII-14. Normalized Raman spectrum of diamond coatings deposited on tungsten rod substrate (same run as in Figs. PII-11 and PII-12). (Courtesy of Dr. T. Haslett, Photonics Research Ontario, Toronto, Canada.)

cence peaking somewhere in the region of 2000 cm^{-1}. Many also display a weak broad peak in the 1500 cm^{-1} region, with only the L1-P4-H4 sample showing strong evidence of graphitic carbon. Samples L3-P4-H8 and L7-P3-H12 appear to have a weak contribution from graphitic carbon. It can be concluded that the films on tungsten tips are very similar throughout the reactor.

3.4. Mo Substrate

Results very similar to those for W substrates were obtained for Mo substrates. Fig. PII-15 shows the normalized spectra obtained. In the case of Mo-substrate spectra, the bores show evidence of the presence of graphitic carbon from positions L1-P4-H9 and L10-P4-H5. Similar to the results for the tungsten substrates, molybdenum substrates do not exhibit significant differences either in the Raman spectra as a function of position in a reactor chamber.

3.5. Stainless steel substrate compared to Mo substrate

A comparative analysis involving both Mo and SS substrate rods with diamond coatings deposited in the same 20-h run was performed to observe differences between the

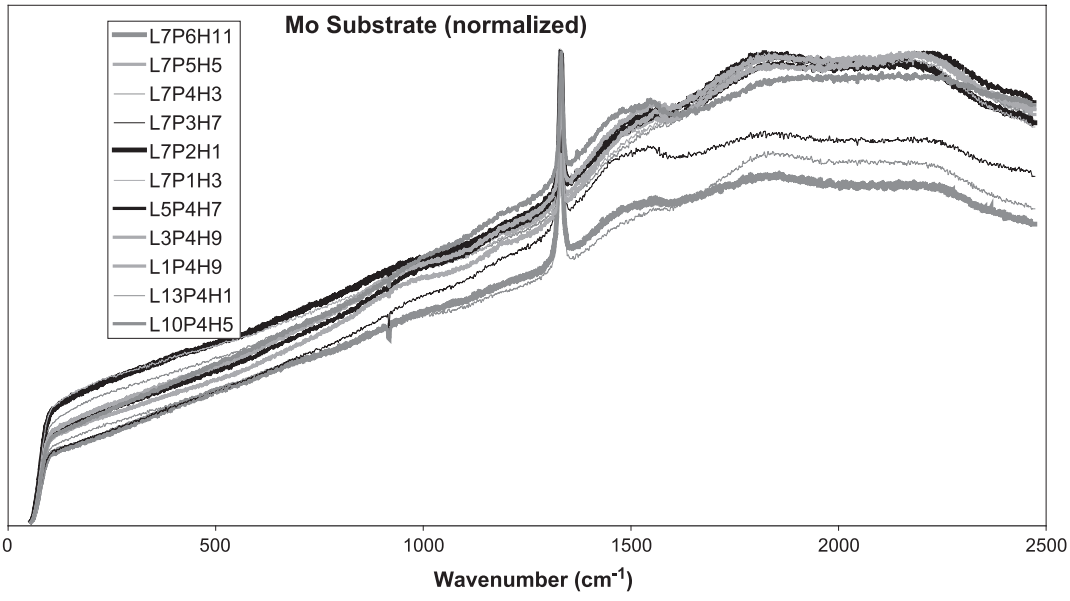

Fig. PII-15. Normalized Raman spectrum of diamond coatings deposited on molybdenum rod substrate (same run as in Figs. PII-11 and PII-12). (Courtesy of Dr. T. Haslett, Photonics Research Ontario, Toronto, Canada).

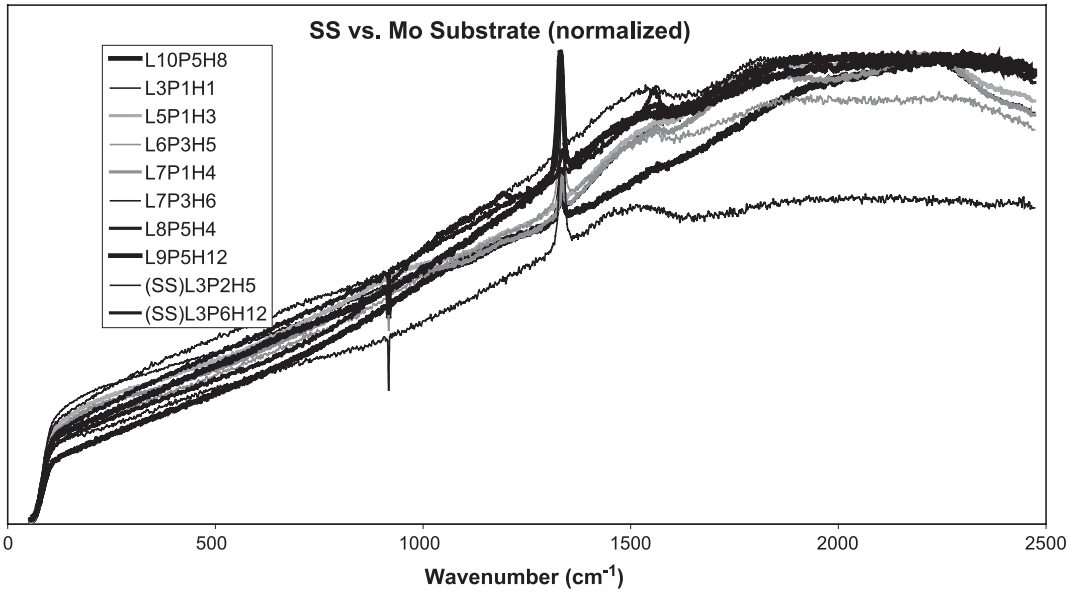

Fig. PII-16. Normalized Raman spectrum of diamond coatings deposited on stainless steel rods vs. molybdenum rod substrates (same run as in Figs. PII-11 and PII-12). (Courtesy of Dr. T. Haslett, Photonics Research Ontario, Toronto, Canada).

two substrates. Fig. PII-16 shows the normalized spectra from this series of rod tips. In this case, unlike other coatings, a significant difference was observed in the uniformity of four of the films on Mo rods and both SS rods. The first four Mo rods displayed relatively uniform films similar to all earlier bores. However, the latter four rods showed sparse carbon-based particulate deposit and larger regions of metal oxide attributed to initial cracks in the metal substrates. Spectra were collected only from carbon-covered regions, but it should be noted that the spectra are not indicative of the overall tip spectrum as most of the tip was uncoated for a few samples. The tips for the SS rods were largely uncoated, with the carbon being present in relatively large particles concentrated mostly near the edge of the tip and down the sides of the rod, although there were particles in the central regions of the tips (see Fig. PII-11).

The spectra from one of the SS rod deposits (L3-P6-H12) show the most distinct spectrum yet observed, with a highly evident graphitic peak and another carbon peak at ~1200 cm^{-1} along with a weak diamond peak. The underlying fluorescence, however, remains very similar to other spectra. Furthermore, the second SS bore displays a spectrum indistinguishable from the other rods in the deposition. Again, there was no indication to suggest the relationship between the rod position and the resulting

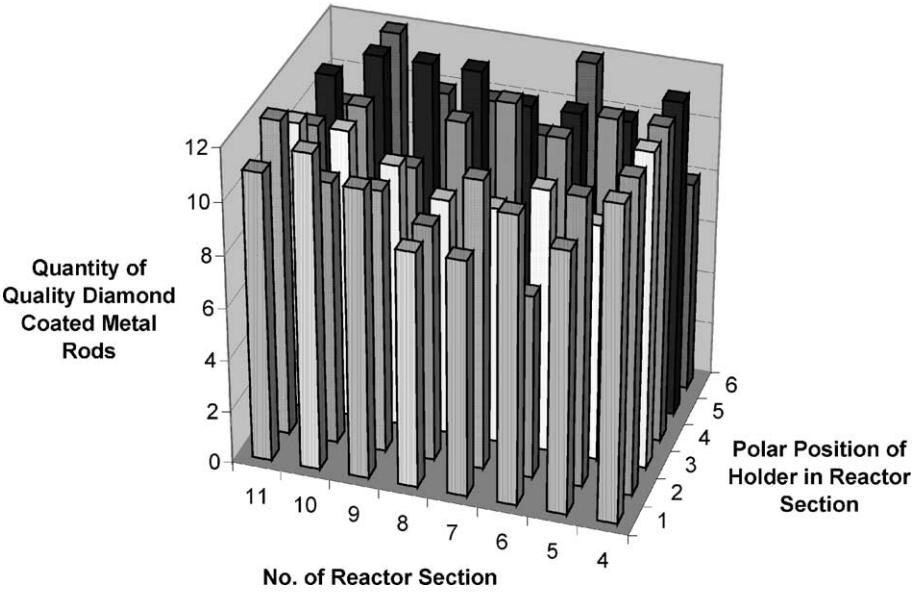

Fig. PII-17. Yield of diamond coated metal rods (same run as in Figs. PII-11 and PII-12).

Table 3
Test parameters for cutting molybdenum glass by carbide burs with different coatings (per one cut)

Test parameter	Value
Rotation speed, rpm	30,000
Load, N	0.7
Time, s	30
Depth of cut, m	0.0008

film nor is there a relationship between the poor Mo-substrate deposits and position.

The Raman spectra analysis as well as comparison of SEM images of diamond films deposited on tungsten and molybdenum rods located at various positions randomly distributed throughout the reaction zone provides no evidence that the film quality or character depends on the position of the rod substrates within the deposition chamber. Raman spectra analysis of carbon crystals positioned on the tip of stainless steel rods revealed that the majority of the crystals have the same diamond-type spectra as the diamond coatings on tungsten and molybdenum. At the same time, few crystals appeared to be non-diamond-carbon phase. This may be explained by the presence of regions in which the PVD TiN/W buffer interlayer is too thin or delaminated. An additional explanation for the presence of non-diamond-carbon phase is the graphitisation of diamond crystals as a result of overheating due to poor contact thermal resistance between the diamond crystals and the stainless steel substrate.

Finally, the uniformity and quality of diamond coating for the 600 metal rod substrates processed in the 20-h CACVD reactor run were profiled by visual inspection using reflective optical microscopy. The results shown in Fig. PII-17 indicate that the production yield of high-quality diamond coating exceeds 85%.

3.6. Testing diamond-coated metal rod substrates for cutting performance

The testing for the cutting performance of the dental burs with diamond coating deposited in the CACVD reactor was conducted by cutting molybdenum glass by a dental turbine handpiece equipped with solid carbide burs having different coatings. The cutting parameters are shown in Table 3. The cutting distance was measured for each type of coating. Comparative results of wear resistance testing of CACVD polycrystalline diamond dental burs with different coatings are shown in Fig. PII-18. The relative wear rate shown in this chart is the ratio: $w'(n)=\mathrm{d}w^{c}(n)/\mathrm{d}w(n)$, where $\mathrm{d}w^{c}(n)/\mathrm{d}w(n)$ is the wear rate of the sample bur subjected to n cuts into the molybdenum glass (each cut had the same 40-mm track length, the same rotation speed and load of the instrument as shown in Table 3), superscript index "c" corresponds to the burs with different coatings. Therefore, $w'(n)$ represents a relative wear rate compared with standard uncoated solid carbide burs. It can be seen that burs with CACVD diamond coatings exhibit a dramatic decrease in wear rate compared to other types of coatings. This is in agreement with observations made from testing diamond-coated tungsten on rolling micro-abrasion in Ref. [20].

4. Conclusions

The CACVD reactor is capable of producing high-quality diamond coatings to accommodate high-volume production. This reactor has demonstrated the ability to deposit polycrystalline diamond coatings with high uniformity and industrial-scale productivity.

Precise control of plasma parameters as well as thermal management of substrates allows for optimization of coating

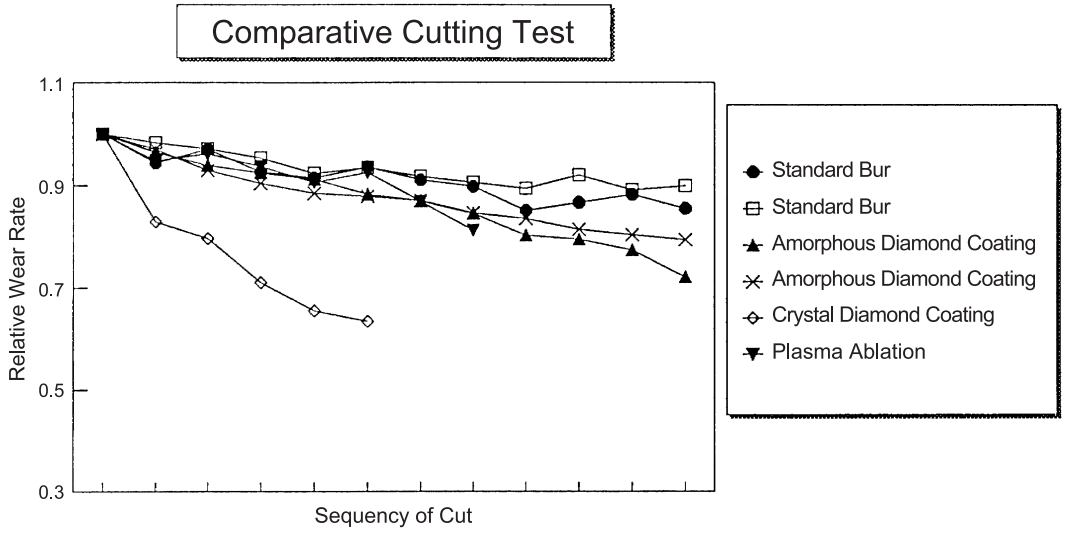

Fig. PII-18. Results of comparative cutting test of solid carbide burs with different coatings for cutting molybdenum glass at 30,000 rpm. (Courtesy of S. Kohnen, Beaver, Canada).

deposition on substrates of different materials having various geometries.

It was also found that direct modification of substrate material by thermal–chemical treatment or depositing diffusion-barrier coatings allows for improvement of CACVD processing of diamond coatings at higher substrate temperatures by blocking the carbon diffusion into the substrate. But both ways require further work to be completed.

Acknowledgements

The work reported in this paper was supported in part by grant from the NRC Canada IRAP Project No. 314901. Much credit is due to C. Bent for administrative support and valuable advice. Equipment engineering and technical assistance was provided by V. Donin and O. Popov. The deposition experiments and design of temperature measurement devices were prepared by M. Shinlov. Their enthusiastic support and assistance in this project are gratefully acknowledged. Raman analysis was conducted by X. Go and T. Haslett of Photonics Research Ontario. Thanks are also due to D. Bhat, A. Inspector and R. Sussman for fruitful discussions, supply of various samples and coating analysis. Their support and assistance in this project are highly appreciated. F. Neub provided assistance with SEM and metallurgical analysis. Special thanks to P. Gannon and R. Smith for assistance in preparing this manuscript.

References

[1] T. Leyendecker, O. Lemmer, S. Esser, M. Frank, in: A. Feldman, Y. Tzeng, W.A. Yarbrough, M. Yoshikawa, M. Murakawa (Eds.), Application of Diamond Films and Related Materials: III Int. Conf., 1995, p. 183.
[2] F.P. Doty, W.A. Jesser, in: R. Messier, J. Glass, J. Butler, R. Roy (Eds.), New Diamond Science and Technology, Mater. Res. Soc. Proc., Pittsburgh, PA, 1991, p. 455.
[3] Li Hou, M. Mecray, W. Yarbrough, X.H. Wang, in: R. Messier, J. Glass, J. Butler, R. Roy (Eds.), New Diamond Science and Technology, Mater. Res. Soc. Proc., Pittsburgh, PA, 1991, p. 461.
[4] K.V. Ravi, A. Joshi, H.S. Hu, in: R. Messier, J. Glass, J. Butler, R. Roy (Eds.), New Diamond Science and Technology, Mater. Res. Soc. Proc., Pittsburgh, PA, 1991, p. 391.
[5] I. Gousman, A. Hoffman, Diamond and Related Materials 7 (1998) 209.
[6] Scott W. Reeve, Wayne A. Weimer, Thin Solid Films 253 (1994) 103.
[7] L.M. Stals, M. Nesladek, C. Quaehaegens, Surface and Coatings Technology 91 (1997) 230.
[8] N. Novikov, V. Gorokhovsky, Uryukov, Surface and Coatings Technology 47 (1991) 770.
[9] Vladimir I. Gorokhovsky, Rabi Bhattacharya, Deepak G. Bhat, Surface and Coatings Technology 140 (2) (2001) 82.
[10] K. Saijo, M. Yagi, K. Shibuki, S. Takatsu, Surface and Coatings Technology 47 (1991) 646.
[11] Hideaki Maeda, Seiji Masuda, Katsuki Kusakabe, Shigeharu Morooka, Diamond and Related Materials 2 (1993) 758.
[12] S.H. Kim, Y.S. Park, J.-W. Lee, Thin Solid Films 253 (1994) 109.
[13] Joral Patschneider, Baybars Oral, Thin Solid Films 253 (1994) 114.
[14] T. Takarada, H. Takezawa, N. Nakagawa, K. Kato, Diamond and Related Materials 2 (1993) 323.
[15] J. Oakes, X.X. Pan, R. Haubner, B. Lux, Surface and Coatings Technology 47 (1991) 600.
[16] Qi hua Fan, A. Fernandes, J. Gracio, Diamond and Related Materials 7 (1998) 603.
[17] M.D. Drory, in: A. Feldman, Y. Tzeng, W.A. Yarbrough, M. Yoshikawa, M. Murakawa (Eds.), Application of Diamond Films and Related Materials: III Int. Conf. 1995, 1995, p. 313.
[18] Vladimir J. Trava-Airoldi, Joao R. Moro, Evaldo J. Corat, Elaine C. Goulart, Ana P. Silva, Nelia F. Leite, Surface and Coatings Technology 108–109 (1998) 437.
[19] Kenji Kobayashi, Nobuki Mutsukura, Yoshio Machi, Tomoyasu Nakano, Diamond and Related Materials 2 (1993) 278.
[20] K. Bose, R.J.K. Wood, Diamond and Related Materials 12 (3–7) (2003) 753.
[21] P.S. Weiser, S. Prawer, D.N. Jamieson, R.R. Manory, Thin Solid Films 290–291 (1996) 186.
[22] G. Verven, Th. Priem, S. Paidassi, F. Blein, L. Bianchi, Diamond and Related Materials 2 (1993) 468.
[23] Naoto Ohtake, Masanori Yoshikawa, Kunio Suzuki, Shin Takeuchi, in: Y. Tzeng, M. Yoshikawa, M. Murakawa, A. Feldman (Eds.), Application of Diamond Films and Related Materials, Elsevier, 1991, p. 431.
[24] H. Chen, M.L. Nielsen, C.J. Gold, R.O. Dillon, J. DiGregorio, T. Furtak, in: Y. Tzeng, M. Yoshikawa, M. Murakawa, A. Feldman (Eds.), Application of Diamond Films and Related Materials, Elsevier, 1991, p. 137.
[25] R.J. Nemanich, L. Bergman, Y.M. Legrice, R.E. Shroder, in: R. Messier, J. Glass, J. Butler, R. Roy (Eds.), New Diamond Science and Technology, Material Research Society, Pittsburgh, PA, 1990, p. 741.
[26] J.G. Buijnsters, P. Shankar, W.J.P. van Enckevor, J.J. Schermer, J.J. ter Meulen, Diamond and Related Materials 11 (10) (2002 October) 1760.
[27] Yongqing Fu, Bibo Yan, Nee LamLoh, Surface and Coatings Technology 130 (2–3) (2000 21 August) 173.
[28] M. Nesladek, K. Vandierendonck, C. Quaehyaegens, M. Kerkhofs, L.M. Stals, Thin Solid Films 270 (1995) 184.
[29] Y.H. Chiou, C.T. Hwang, M.Y. Han, J.H. Jou, Y.S. Chang, H.C. Shih, Thin Solid Films 253 (1994) 119.
[30] J. Stiegler, S. Roth, K. Hammer, O. Stenzel, B. Mainz, W. Scharff, Diamond and Related Materials 2 (1993) 413.
[31] V. Gorokhovsky, US Patent No. 6,684,759.